# Dual-polarized inverted quad-ridged flared horn antenna with one decade bandwidth for OTA testing

Zhang, Xue; Wang, Zhengpeng; Pan, Chong; Ba, Xinran; Wang, Yi

*DOI:*
10.1109/LAWP.2022.3162337

# Dual-Polarized Inverted Quad-Ridged Flared Horn Antenna with One Decade Bandwidth for OTA Testing

Xue Zhang, Zhengpeng Wang, *Member, IEEE*, Chong Pan, Xinran Ba, and Yi Wang, *Senior Member, IEEE*

***Abstract*—This paper presents a dual-polarization inverted quad-ridged flared horn antenna with an extremely wideband of more than one decade in the range of 2-20 GHz. The modes of the inverted quad-ridged waveguide are analyzed first. A cross-shaped inverted ridge, with low $TE_{11}$ mode cutoff frequency and a tip significantly higher than the horn aperture, is proposed. The inner surface of the horn wall is based on a composite curve flare rate. It is optimized to cooperate with the inverted ridge. Furthermore, the PTFE back cavity replaces metal back cavity to suppress the high order mode in the back cavity. The measured isolation between the two orthogonal linearly-polarized ports is nearly 45 dB and the reflection coefficient is less than -15 dB over the entire working frequency band.**

***Index Terms*—Inverted Quad-Ridged Flared Horn, Ultra-Wide Band, High Ports Isolation, Balanced Feed, OTA.**

## I. Introduction

Ultra wideband (UWB) high performance probe antenna is critical for improving over-the-air (OTA) test efficiency. Quad Ridged Horn (QRH) antenna is a directional antenna with wide bandwidth and dual polarization performance [1-5]. Many excellent works have been done to improve the working bandwidth and radiation pattern performance of the QRH[6-8].

Recently, balanced feed structure has attracted lots of attention [9-11]. Zhao *et al.*[10] reported a balanced feed QRH. The significant advantage of the design is the reduced sensitivity of VSWR to manufacturing errors. Foged *et al*. use an inverted quad-ridged structure to provide four rotation-symmetrical feeding points for external balanced feeding [11]. The inverted quad-ridged horn shows good matching, high isolation, and low cross polarization performance with 1.5:1 bandwidth. This paper analyzes the propagation modes of the inverted QRH along the length of the horn antenna. An optimized inverted QRH with a tip higher than the horn aperture is then proposed. The PTFE back cavity replaces metal back cavity to suppress the high order mode in the back cavity. The main lobe radiation pattern keeps stable in the whole working frequency band.

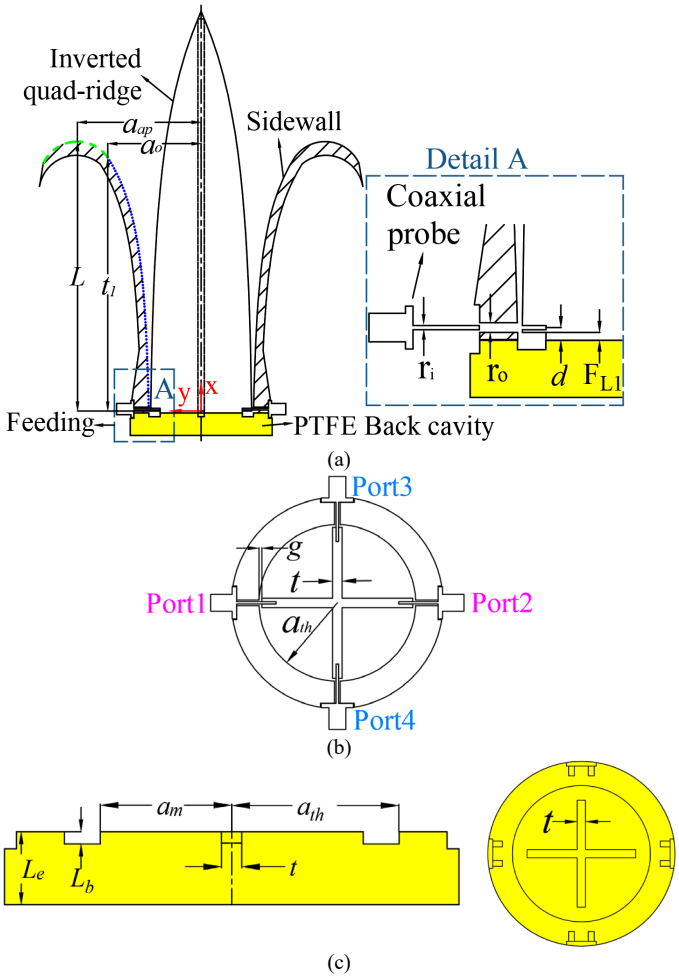


Fig. 1. (a) The profile of the IQRFH antenna. (b) The cross-section view at the feed position of the IQRFH. (c) The profile and top view of the PTFE back cavity.

This work is supported by the Beijing Municipal Science and Technology Project under Grant Z191100007519002 (Corresponding author: Chong Pan).

Xue Zhang, Zhengpeng Wang are with the Electromagnetic Laboratory, School of Electronic and Information Engineering, Beihang University (BUAA), Beijing 100191, China (email: zhangxue9701@qq.com; wangzp@buaa.edu.cn).

Xinran Ba is with State Key Laboratory of Media Convergence and Communication, Communication University of China, Beijing, China.

Chong Pan is with China Academy of Information and Communications Technology, Beijing, China.

Yi Wang is with Department of Electronic, Electrical and Systems Engineering, University of Birmingham, Edgbaston, Birmingham, B15 2TT, United Kingdom (email: Y.Wang.1@bham.ac.uk).

To the best of our knowledge, directional antennas with balanced feed structure covering one-decade bandwidth have not been reported before. This paper presents a balanced fed dual-polarized inverted quad-ridged flared horn (IQRFH) (shown in Fig. 1) operating at 2 – 20 GHz with high port isolation and low reflection coefficient.

## II. Antenna Configuration

The IQRFH is divided into two parts: the feeding network and the radiation section. All the parameters that define IQRFH are determined by the design rules discussed in section III.

### A. Feeding Network

Four subminiature version A (SMA) coaxial probes are symmetrically distributed around the horn side wall, as shown in Fig. 1. The outer conductors of the coaxial probes are attached to the sidewall of the horn, and the inner conductors are inserted into the inverted quad-ridge. The inset 'Detail A' in Fig. 1(a) shows the diameters of the inner and outer conductors of the coaxial probes: $r_i$ = 1.27 mm, and $r_o$ = 2.92 mm. The parameter $d$ represents the distance between the center of the coaxial probe and the bottom of the inverted quad ridge. Fig. 1(b) shows the cross-section view at the feed position of the IQRFH. The balanced feed is achieved by feeding differential signals to a pair of opposite ports. The differential signals are generated by a 180° hybrid coupler [12]. The radius of the inverted quad-ridged waveguide (IQRWG) at the feeding point, $a_{th}$, the ridge thickness $t$, and the gap width $g$ between the ridge and the sidewall are shown in Fig. 1(b). The optimized values are $d$ =2 mm, $a_{th}$ =28 mm, $t$ =3.4 mm, and $g$ =1 mm.

Fig. 1(c) shows the back cavity. It is noteworthy that the back cavity is made of polytetrafluoroethylene (PTFE), which has an extremely low dielectric constant. The cross-shaped dielectric block located in the center of the cavity supports the inverted quad-ridge. Both the cross-shaped dielectric block and the inverted quad-ridge have the same cross section. The parameters of the back cavity are given in Table I.

### B. Radiation Section

The radiation section consists of the tapering inverted quad-ridge and flared sidewall. The inverted quad-ridge is the cross conductor in the center of the flared horn, which can be divided into three sections: $S_1$, $S_2$, and $S_3$, as shown in Fig. 2. To insert the coaxial probe into the inverted quad-ridge, S1 contains two parts with constant cross-section along the x-direction, with lengths $F_L$ and $F_{L1}$, respectively. The parameter $F_{L1}$ is shown in Fig.1(a). $S_2$ employs an exponential curve to create a smooth profile. Fig. 2 shows the coordinate axes. The exponential curve (the blue bold curve in Fig. 2) is defined as:

$$y_1 = c_1 e^{kx_1} - c_1 \qquad 0 \le x_1 \le t_0 \tag{1}$$

where $c_1$ =0.9, $k$ =0.0163, $t_0$ =208.816.

Furthermore, $S_3$ is a pyramid located at the tip of the inverted quad-ridge. The width and length of the ridge are $R_W$ and $R_L$, respectively. The values for the geometrical parameters are as follows: $F_L$ =2 mm, $F_{L1}$ =1 mm, $R_W$ =54 mm, and $R_L$ =213 mm.

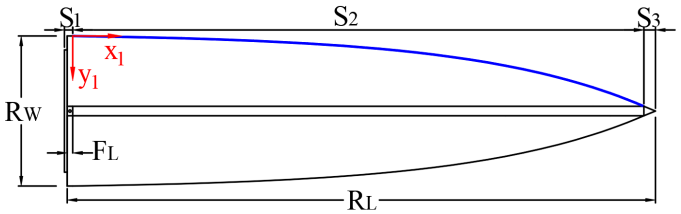


Fig. 2. The side view of the inverted quad-ridge.

The profile of the sidewall follows the design from Akgiray *et al.* [6]. As shown in Fig. 1(a), the sidewall profile is composed of an exponential curve (the blue dotted curve) and an elliptical curve (the green dashed curve). The coordinate axes that define these two curves are shown in Fig. 1(a). The exponential curve is defined as:

$$y = A\left(c_3 e^{Rx} + c_4\right) + (1-A)\left(a_{th} + (a_o - a_{th})\frac{x}{t_1}\right) \tag{2}$$

$$c_3 = \frac{a_o - a_{th}}{e^{Rt_1} - 1}\ , c_4 = \frac{a_{th}e^{Rt_1} - a_o}{e^{Rt_1} - 1} \tag{3}$$

where $a_o$ is the sidewall radius at the end of the exponential curve; $R$ is the exponential opening rate and $t_1$ is the taper length. The parameter $A \in [0,1]$ determines whether a linear taper is added. The value of variable $x$ ranges from 0 to $t_1$.

The elliptical curve joins the end of the exponential curve. It is defined as:

$$x = a_e \sin\alpha\cos\theta + b_e \cos\alpha sin\theta - b_e sin\theta + t_1 \tag{4}$$

$$y = a_e \sin\alpha\cos\theta - b_e \cos\alpha sin\theta + b_e sin\theta + a_o \tag{5}$$

where $a_e$, $b_e$ are the major and minor axes of the ellipse, respectively; $\theta$ is the half flare angle; $\alpha$ is the ellipse sweep angle from 0° to $\alpha_s$ [13]. The aperture of the horn is $a_{ap}$ and the length of the sidewall is $L$. In addition, all remaining parameters of the sidewall are listed in Table I.

TABLE I Parameters of the IQRFH (Unit: mm/rad)

| Parameters | Value | Parameters | Value | Parameters | Value |
|---|---|---|---|---|---|
| A | 0.9 | $b_e$ | 20 | $a_{th}$ | 28 |
| R | 0.031 | θ | π/2 | $L_b$ | 2 |
| $\alpha_s$ | 2π/3 | $a_{ap}$ | 66.37 | L | 143.5 |
| $t_1$ | 135 | $a_o$ | 50 | $L_e$ | 12 |
| $a_e$ | 20 | $a_m$ | 22 | | |

## III. Antenna Design Rules

The three-step design procedure of the IQRFH is described first, followed by the detailed explanation. The three steps in the design are as follows:

1) Determine the size of the IQRWG at the feeding point, shown in Fig. 1(b), according to the required cutoff frequency.

2) Design the inverted quad-ridge and the sidewall to achieve low reflection coefficient in wide band and desirable radiation performance.

3) Design dielectric back cavity to support the inverted quad-ridge and reduce backward radiation.

### A. IQRWG Mode Analysis

The modes of the IQRWG are calculated and analyzed in CST Microwave Studio. It is noted that only odd modes are excited in this design. In Fig. 3, the cutoff frequencies of $TE_{11}$, $TM_{11}$, $TE_{31}$, and $TE_{12}$ are depicted for an IQRWG with a radius $a_{th}$ = 28 mm, the ridge thickness $t$ = 3.4 mm, and varying ridge

to sidewall gap, $g$. The small gap, $g$, with fixed $a_{th}$ lowers the cutoff frequency of the dominant $TE_{11}$ mode and increases the separation between the $TE_{11}$ mode and the unwanted higher order modes. It is critical to choose an adequately small value of $g$ to achieve broadband. The choice of the radius $a_{th}$ is determined by the required cutoff frequency of the $TE_{11}$ mode, which is 1.02 GHz, in this case. This is the lowest achievable cutoff frequency as shown in Fig. 3. According to the simulation study, the ridge thickness $t$ should be evaluated around 0.1 $\lambda_m$, where $\lambda_m$ is the wavelength at the center frequency of 11 GHz.

### B. Design Rules for Inverted Quad-Ridge and Sidewall

The tapering ridge and the flared sidewall collectively ensure a smooth impedance transmission from the IQRWG to the free space, and these need to be optimized to achieve broadband.

The length of the ridge is a key factor in achieving a low reflection coefficient and acceptable radiation performance over the entire frequency band. To illustrate this, three ridges of different lengths are studied. Fig. 4(b) shows the three ridge profiles with all other parameters fixed, referred to as Horn1, Horn2, and Horn3. The lengths of the ridges of Horn2 and Horn3 are reduced by 25% and 50% respectively from that of Horn1. The cutoff frequency of the dominant mode and some higher order modes along the axis of the horn were calculated. The results are plotted in Fig. 4(a).

The short ridge implies a large exponential opening rate, $k$, which causes the cutoff frequency of the dominant $TE_{11}$ mode to increase rapidly (refer to the case of Horn3) and result in the deterioration of the reflection coefficient at low frequency. It also leads to a lower cutoff frequency of $TM_{11}$ mode than that of Horn1 and Horn2. The tips of the ridges for Horn1 and Horn2 are higher than the horn aperture. The cutoff frequencies of their $TE_{11}$ mode are relatively constant, while the cutoff frequencies of the $TM_{11}$ mode are higher than that of Horn3.

The length $R_L$ of the ridge of Horn1 is approximately $1.4\lambda_c$ (cut-off wavelength) and the tip of the inverted ridge is $0.46\lambda_c$ higher than the horn aperture. The longer ridge can further decrease the working frequency without deteriorating the radiation performance.

### C. Design of the Back Cavity

The back cavity of the conventional quad-ridged horn antenna is made of metal. However, high-order modes are excited in the proposed IQRFH due to the very wide working bandwidth which causes radiation pattern notches at some specific frequencies. Therefore, a dielectric back cavity is employed to fix the inverted ridges in the structure and suppress the high-order mode. Fig. 5 compares simulated antenna gain with a metal back cavity and that with a dielectric back cavity. It can be observed that the gain notches are removed by using PTFE back cavity. The simulated gain does not include the hybrid couplers. The hybrid couplers incur extra loss in the gain measurement.

The dimension $a_m$ of the PTFE block has a strong influence on the reflection coefficient, a good reflection coefficient can be obtained when the parameter $a_m$ is set to 22 mm.

## IV. Simulation and Measured Results

A prototype is manufactured to demonstrate the proposed concept, as shown in Fig. 6. The scattering parameters and radiation patterns were measured in an anechoic chamber using the network analyzer.

### A. Scattering Parameters

The simulated and measured scattering parameters of both polarizations of the IQRFH, including the couplers for differential feeding are presented in Fig. 7. The simulated and measured scattering parameters are generally consistent. The simulated S11 and S22 are identical owing the rotational symmetry of the structure. It can be seen that the measured $S_{11}$ and S22 are below -15 dB over 10:1 bandwidth. The measured S21 (isolation) is higher than 45 dB across all of the operating frequency band. High isolation between the two orthogonal linearly polarized ports is obtained.

### B. Radiation Patterns

The simulated and measured co-polarized and

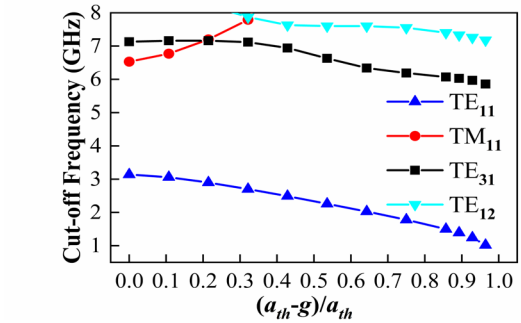


Fig. 3. Cutoff frequencies of the odd modes in the IQRWG.

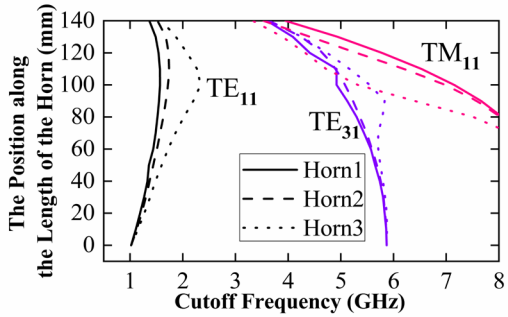


(a)

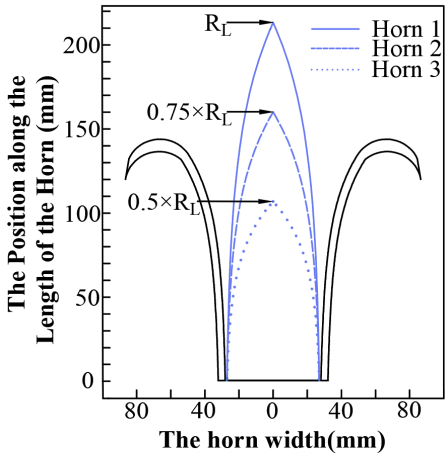


(b)

Fig. 4. The cutoff frequency of the mode calculated from the horns with different cone ridge profiles in (b) is given in (a).

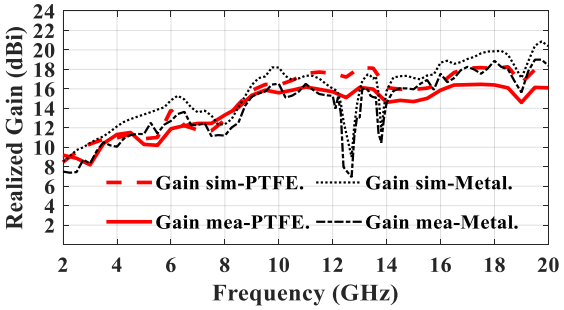


Fig. 5. The realized gain of the IQRFH.

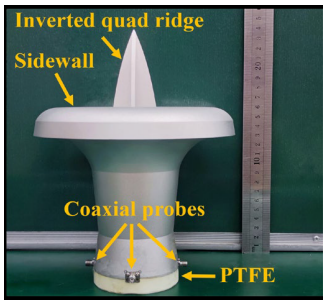


Fig. 6. Photograph of the balanced-fed IQRFH prototype.

cross-polarized radiation patterns are shown in Fig. 8. Considering the rotational symmetry of the entire horn structure, only the simulation and measured results of one polarization are given.

### *C. Performance Comparison*

The comparison between the proposed IQRFH and other published QRHs is presented in Table II. The proposed IQRFH exhibits the best overall performance in terms of one decade bandwidth, low reflection coefficient, the highest isolation, and radiation pattern performance. Reasonable gain and relatively low cross polarization are also achieved.

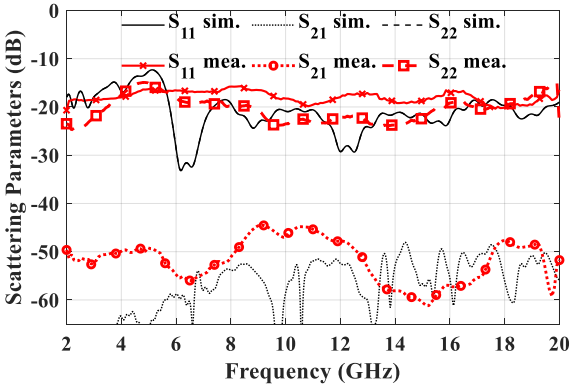


Fig. 7. The measured and simulated scattering parameters of the IQRFH.

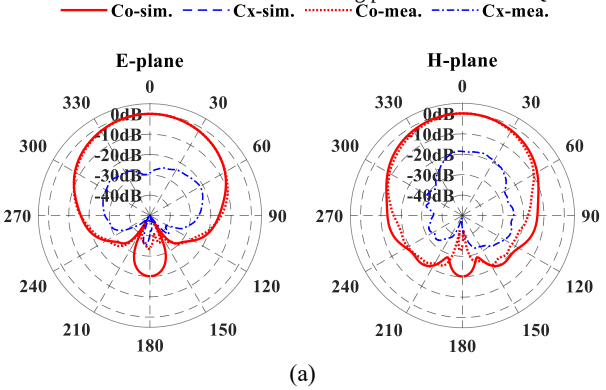


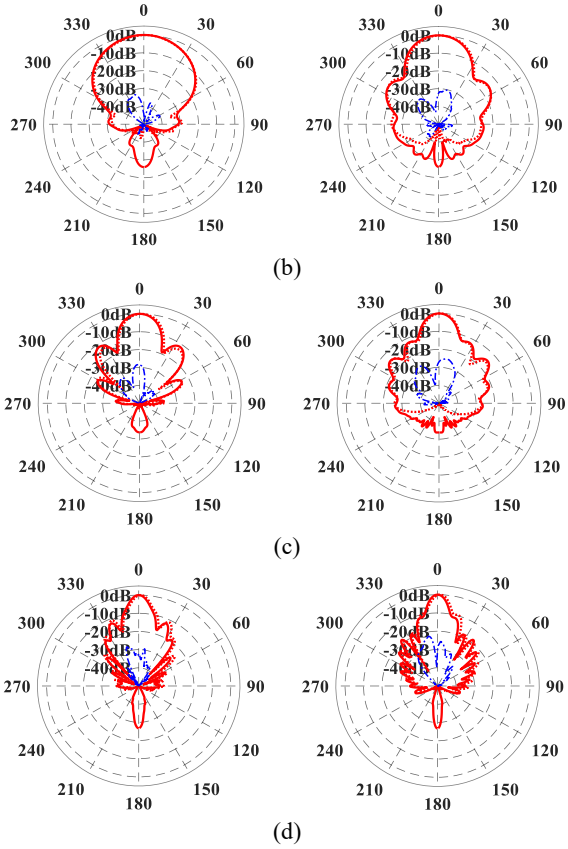


Fig. 8. Simulated and measured radiation patterns of the IQRFH. (a) 2 GHz (b) 5 GHz (c) 10 GHz (d) 20 GHz.

TABLE II COMPARISON BETWEEN THE PROPOSED IQRFH AND OTHER PUBLISHED DESIGNS.

| Ref. | Bandwidth (GHz) | S11 (dB) | Isolation (dB) | Gain (dBi) | Balanced feed | Split radiation pattern |
|---|---|---|---|---|---|---|
| [1] | 1.95-19.35 (9.9:1) | -7.36 | 41# | 5.7-20.28 | No | Yes |
| [11] | (1.5:1) | -10 | 55 | / | Yes | No |
| [14] | 2.4-24 (10:1) | -10* | 25 | 10.5-21.1 | No | Yes |
| [15] | 4.6-24 (5.2:1) | -10* | Around 25 | N/A | No | / |
| [16] | 1.5-15.5 (10.3:1) | -7 | 35 | 6.5-12.5 | No | Yes |
| [17] | 1-6.75 (6.75:1) | -10 | 28# | 13.6-18.1 | No | / |
| This work | 2-20 (10:1) | -15 | 45 | 8.2-16.47 | Yes | No |

* The reflection coefficient exceeds the quoted value at some frequency points.
# Simulated result.

## V. CONCLUSION

A dual polarized IQRFH with an ultra-wide bandwidth over 10:1 is demonstrated. The cutoff frequency of the mode versus the ratio of radius to gap in the IQRWG is analyzed. The ridges of different lengths were analyzed to illustrate the effect on low-frequency performance. Finally, the high order harmful resonant modes are suppressed by using the dielectric back cavity which improves radiation pattern performance.

A prototype of the proposed IQRFH is manufactured and measured. Excellent agreement between measurement and simulation results has been achieved.

## REFERENCES


[1] L. Chang, L. Chen, J. Zhang, and D. Li, "A 1.95-19.35 GHz quad-ridge horn antenna with stable unidirectional radiation patterns," in 2018 12th International Symposium on Antennas, Propagation and EM Theory (ISAPE), 2018, pp. 1-3.

[2] J. Shang, C. Lv, X. Luo, and C. Fan, "A novel dual-polarized broadband feed for the compact range application," in 2019 International Symposium on Antennas and Propagation (ISAP), 2019, pp. 1-3.

[3] A. Giacomini, A. Potenza, R. Morbidini, and L. Foged, "Quad-ridge dual polarized antenna for use in the 2–32GHz band," in 2012 6th European Conference on Antennas and Propagation (EUCAP), 2012, pp. 769-772.

[4] S. Zhongxiang and F. Chao, "A new dual-polarized broadband horn antenna," IEEE Antennas Wireless Propag. Lett., vol. 4, pp. 270-273, 2005.

[5] R. Dehdasht-Heydari, H. R. Hassani, and A. R. Mallahzadeh, "A new 2-18 GHz quad-ridged horn antenna," Progress in Electromagnetics Research-Pier, vol. 81, pp. 183-195, 2008 2008.

[6] A. Akgiray, S. Weinreb, W. A. Imbriale, and C. Beaudoin, "Circular quadruple-ridged flared horn achieving near-constant beamwidth over multioctave bandwidth: Design and measurements," IEEE Trans. Antennas Propag., vol. 61, no. 3, pp. 1099-1108, Mar. 2013.

[7] O. B. Jacobs, J. W. Odendaal, and J. Joubert, "Quad-ridge horn antenna with elliptically shaped sidewalls," IEEE Trans. Antennas Propag., vol. 61, no. 6, pp. 2948-2955, Jun. 2013.

[8] F. Oktafiani, E. Y. Hamid, and A. Munir, "- performance evaluation of quad-ridged horn antenna in variation of its ridge profile," vol. -, no. -, pp. - 217, 2019.

[9] T. S. Beukman, M. V. Ivashina, R. Maaskant, P. Meyer, and C. Bencivenni, "A quadraxial feed for ultra-wide bandwidth quadruple-ridged flared horn antennas," in The 8th European Conference on Antennas and Propagation (EuCAP 2014), 2014, pp. 3312-3316.

[10] Z. Zhao and Z. Wang, "A balanced feed quad-ridged horn antenna," in 2019 13th European Conference on Antennas and Propagation (EuCAP), 2019, pp. 1-4.

[11] L. J. Foged, A. Giacomini, R. Morbidini, and A. Potenza, "Wideband field probes for advanced measurement applications," in 2011 IEEE International Conference on Microwaves, Communications, Antennas and Electronic Systems (COMCAS 2011), 2011, pp. 1-7.

[12] http://www.qotana.com/pdf/id/152/mod/Hybrid

[13] Z. Wang, P. S. Hall, J. R. Kelly, and P. Gardner, "Wideband frequency-domain and space-domain pattern reconfigurable circular antenna array," IEEE Trans. Antennas Propag., vol. 65, no. 10, pp. 5179-5189, Oct 2017.

[14] Y. Ma et al., "A 10:1 bandwidth cryogenic quadruple-ridged flared horn design for reflector antennas in radio astronomy," IEEE Access, vol. 8, pp. 81101-81115, 2020.

[15] B. Dong, J. Yang, J. Dahlstrom, J. Flygare, M. Pantaleev, and B. Billade, "Optimization and realization of quadruple-ridge flared horn with new spline-defined profiles as a high-efficiency feed from 4.6 GHz to 24 GHz," IEEE Trans. Antennas Propag., vol. 67, no. 1, pp. 585-590, Jan 2019.

[16] J. Flygare and M. Pantaleev, "Dielectrically loaded quad-ridge flared horn for beamwidth control over decade bandwidth—optimization, manufacture, and measurement," IEEE Trans. Antennas Propag., vol. 68, no. 1, pp. 207-216, 2020.

[17] B. Solak, M. Secmen, and A. Tekin, "The design of a high gain dual-polarized quad-ridged circular horn antenna for wideband emc test applications," Applied Computational Electromagnetics Society Journal, vol. 33, no. 9, pp. 1009-1017, 2018.